AAEC/E648


AAEC/E648

AUSTRALIAN ATOMIC ENERGY COMMISSION
RESEARCH ESTABLISHMENT
LUCAS HEIGHTS RESEARCH LABORATORIES

# MICROSTRUCTURAL ASPECTS OF SYNROC FROM SANDIA PRECURSOR

## 1. SOME EFFECTS OF PROCESS VARIABLES

by

G. T. STEVENS

K. G. WATSON

A. BELLROSE

APRIL 1987

ISBN 0 642 59855 X

AUSTRALIAN ATOMIC ENERGY COMMISSION
RESEARCH ESTABLISHMENT

LUCAS HEIGHTS RESEARCH LABORATORIES

# MICROSTRUCTURAL ASPECTS OF SYNROC FROM SANDIA PRECURSOR

## 1. SOME EFFECTS OF PROCESS VARIABLES

BY

G T STEVENS

K G WATSON

A BELLROSE

**ABSTRACT**

Typical microstructures formed in Synroc C have been observed by optical and scanning electron microscopy. The principal effects of segregation, variation of calciner atmosphere and change in hot-pressing conditions, are summarised.

National Library of Australia card number and ISBN 0 642 59855 X

The following descriptors have been selected from the INIS Thesaurus to describe the subject content of this report for information retrieval purposes. For further details please refer to IAEA-INIS-12 (INIS: Manual for Indexing) and IAEA-INIS-13 (INIS: Thesaurus) published in Vienna by the International Atomic Energy Agency.

BARIUM OXIDES; CALCINATION; CALCINED WASTES; HOLLANDITE; HOT PRESSING; MICROSTRUCTURE; PEROVSKITE; RADIOACTIVE WASTE PROCESSING; RUTILE; SEGREGATION; SYNROC PROCESS; SYNTHETIC ROCKS; TRANSMISSION ELECTRON MICROSCO; ZIRCONOLITE; TITANIUM OXIDES

**EDITORIAL NOTE**

From 27 April 1987, the Australian Atomic Energy Commission (AAEC) is replaced by Australian Nuclear Science and Technology Organisation (ANSTO). Serial numbers for reports with an issue date after April 1987 have the prefix ANSTO with no change of the symbol (E, M, S or C) or numbering sequence.

CONTENTS

## 1. INTRODUCTION

Synroc is a multiphase, fine-grained polycrystalline titanate for the immobilisation of high-level waste (HLW) from the nuclear power industry. As originally conceived, the structure was a relatively simple assemblage of three synthetic minerals [Ringwood 1978]. Although the basic concept remains sound, subsequent microstructural analysis, principally by transmission electron microscopy (TEM), has shown the structure to be exceedingly complex and the fine details have yet to be fully elucidated [Cooper *et al.* 1985].

In association with the Australian National and Griffith Universities, the AAEC is developing techniques for the preparation of a Synroc wasteform for the incorporation of nuclear waste. Material associated with these studies is evaluated by a variety of means, the authors being responsible for determining the structure down to about one micrometre (5000 times magnification).

The principal effects of changing process variables (see **section 2.2**) on the microstructure of one batch of Synroc (Sandia RE15642), observed by optical and scanning electron microscopy, are summarised.

## 2. OUTLINE OF THE FABRICATION PROCESS

### 2.1 Synroc B

The Sandia process for the preparation of Synroc precursor [Dosch *et al.* 1984] involves the hydrolysis of a mixture of sodium hydroxide-methanol solutions of titanium tetra-isopropoxide and zirconium tetra-n-butoxide in acetone-water solution. The sodium titanate/zirconate is then reacted with aluminium, barium and calcium in nitrate solutions which exchange for the sodium. The residual sodium is removed by washing and the material dried to a fine powder. If the precursor is hot-pressed without the addition of nuclear waste, it is termed Synroc B. A typical composition of Synroc B is given in **table 1**.

The Synroc material described in this report was formed from a single delivery of the precursor from a commercial chemical supplier.

### 2.2 Synroc C

In these studies simulated HLW was added to the precursor, generally at a level of 10 per cent, to form Synroc C. The composition of the HLW (US reference simulated waste PW-4b [Mendel *et al.* 1977]) is given in **table 2.**

The preparation of Synroc C in the laboratory involves the following basic steps:

(i) The precursor is slurried in water and the HLW added in a 2*M* solution of $HNO_3$, ammonia being used to maintain the pH at 9.

(ii) The resulting slurry is dried.

(iii) The material is then calcined for one hour at 750°C in an atmosphere of 3.5% $H_2$ in nitrogen.

(iv) Two per cent of titanium metal is added as a fine powder and blended with the calcine (the Ti is used to reduce the redox potential during the hot-pressing).

(v) The material is hot-pressed at about 1200°C and 14 MPa for two hours in a graphite die.

## 3. EXPERIMENTAL

Specimens for microscopy were set in a 25 mm diameter mount of casting resin at room temperature and the surface was ground by hand on silicon carbide papers of successively finer grit. Final polishing was carried out by an automatic polishing machine on a spirally-grooved tin lap (Sirolap) with 4-8 then 0-0.25 micrometre diamond paste and a mineral oil lubricant, for about 20 minutes at each stage.

A thin conducting layer of carbon was evaporated onto the polished surface for examination in the scanning electron microscope. Scanning electron microscopy (SEM) was carried out at 25 kV or 15 kV, followed by electron-probe X-ray energy dispersive (EDS) analysis at 15 kV. The resolution of the electron microprobe, set by penetration and scattering of the electrons, is about one micrometre. When analysing fine crystals of about this size there will be a significant but indeterminate contribution to the spectra from the neighbouring material.

In the case of optical microscopy, the poor contrast of the ceramic phases makes interpretation of the structure difficult. Cracks and voids, however, can be easily detected as dark areas whereas metallic phases

appear bright. Optical microscopy is also useful for detecting certain translucent contaminants which undergo internal reflection and so appear bright in polarised or dark-field illumination.

We have found back-scattered electron (BSE) imaging in the SEM to be a most useful technique as the images show relative contrast according to the average atomic number of the particular phase. Energy dispersive analysis quickly and easily determines the elements present in regions down to a diameter of about one micrometre, so it is possible to use levels of contrast as a rough guide to composition. Secondary electron imaging (SEI), although showing lower atomic number contrast than BSE imaging, is better at revealing such topographical features as cracks and voids.

Although many EDS systems are capable of quantitative analysis, consistent results with Synroc using our system have not been achieved. The main difficulties are the large number of elements present and the overlap of the two main peaks of the Ba spectrum ($L\alpha_1$ at 4.469 eV, $L\beta_1$ at 4.831 eV) with the peaks from Ti($K\alpha_1$ at 4.511 eV, $K\alpha_2$ at 4.504 eV and $K\beta$ at 4.931 eV); this effect is apparent in **figure 2**. It seems that the stability of the instrumentation is not sufficient to allow the computer software to separate the two spectra consistently.

## 4. REFERENCE STRUCTURES

Representative micrographs of the 'best' structures produced from RE15642 Sandia are shown in **figure 1**. The obvious feature in the low magnification micrographs is the dispersion of porous titanium oxide particles (about 50 μm in size) which are relics of the Ti metal added to reduce the redox potential during hot pressing. These are subsequently referred to as Ti(oxide) relics.

High magnification is necessary to resolve the fine grains of the matrix. The matrix phases are nominally

(i) zirconolite ($CaZrTi_2O_7$),

(ii) barium hollandite ($BaAl_2Ti_6O_{16}$),

(iii) perovskite ($CaTiO_3$),

(iv) rutile ($TiO_2$), and

(v) metallic alloy (*e.g.* Mo, Pd, Ru, Fe),

although TEM and other techniques have shown that these ideal compositions are not always achieved in the case of zirconolite, hollandite and rutile [Cooper *et al.* 1985]. The nominal phases are identified in **figure 2** by their X-ray emission spectra (XES). Transmission electron microscopy is capable of revealing much finer detail of the structure.

The morphology of the microconstituents is better shown at lower magnification in **figure 1b**. The appearance is determined by the morphology of the darker rutile or Ti oxide phase. The matrix Ti oxide varies from small equi-axed grains through chains of grains and irregular extended crystals to quite well developed acicular crystals. In the sample batch of Sandia, the mixed (irregular and sharp) acicular structure is common. The other matrix phases show no similar variation and are generally fine, equi-axed grains below one micrometre in size.

## 5. PROCESSING CONTAMINANTS

A variety of contaminants have been occasionally observed in Synroc specimens, the two most common being zirconium oxide particles and stainless steel.

(a) *Zirconium Oxide Particles.* An attrition mill is sometimes employed in the initial slurrying operation and fragments of the zirconia balls can be carried through into the Synroc C. These are readily distinguished from zirconium oxide segregation from other sources by the presence of a small quantity of the stabilising element Mg. An example is shown in **figure 3**.

(b) *Stainless Steel.* Tramp metallic particles from the equipment appear as globular clusters with light SEM contrast. Caesium is often found in these regions associated with Si, a common impurity in steels, which is concentrated in oxide scale. **Figure 4** shows the interaction of stainless steel contamination with the matrix and a Ti(oxide) relic.

## 6. SEGREGATION IN THE SLURRY

Serious segregation in the slurry can give rise to coarse inclusions in the Synroc C which are often internally cracked; this cracking may extend into the matrix of the material. Examples of this phenomenon are shown in **figures 3, 5, 6** and **7**. The segregations are often rich in calcium or barium and present a major difficulty in the preparation of a homogeneous Synroc microstructure.

Calcium and barium segregations have not been observed in Synroc B, so they must be due either to the addition of HLW or to subsequent processing. It is thought that the segregation arises when the acid HLW nitrate solution is added to the precursor. Local acid conditions are presumed to lead to stripping of the Ca and Ba from the precursor substrate and their subsequent migration through the residual liquid to precipitate as hydroxide when basic conditions are restored [A Chetcuti and J L Woolfrey, AAEC unpublished results]. Close control of the HLW addition and drying of the slurry can substantially eliminate this segregation. Reduction in particle size of the dried slurry by hammer milling has been used to reduce the size of these segregates which, in turn, reduces the internal cracking (**figure 7**).

## 7. CALCINATION ATMOSPHERE

Varying the composition of the inlet gas to the calciner from pure nitrogen, through several (low) partial pressures of oxygen in $N_2/H_2$ and $CO/CO_2$ mixtures, to pure hydrogen had little effect on the microstructure except when pure hydrogen was used. The structure then contained relatively large irregular crystals randomly arranged in a fine non-uniform matrix (**figure 8**). Ringwood and Kesson [Australian National University, unpublished results] have identified this new phase as $Ca(Al,Ti)_2Ti_8O_{20}$.

## 8. HOT-PRESSING CONDITIONS

### 8.1 Soaking Time

More porosity was produced in a compact of dense granules when it was held at 1200°C for four hours before the application of pressure (**figure 9**) than when pressure was applied immediately 1200°C was reached.

### 8.2 Hot-pressing Time

Varying the time of application of pressure from 0.5 to two hours had little effect on the microstructure.

### 8.3 Hot-pressing Temperature

As the pressing temperature is increased, a slight increase in grain size occurs (to about one micrometre) until, at a certain temperature, rapid growth of the Ti oxide-based phase takes place. Rapid grain growth in ceramics is attributed to the formation of mobile grain boundaries or liquid films.

At pressing temperatures of around 1290 to 1300°C, the structure typically consists of colonies of mutually aligned, extremely coarse crystals of titanium oxide in a matrix of finer equi-axed grains of the other phases (**figure 10**). Above about 1300°C, extremely large primary crystals of titanium oxide are formed (**figure 11**).

### 8.4 Pressure-Temperature Variation

In a separate study, the hot-pressing conditions were varied over the ranges 1150 - 1250°C and 7 to 21 MPa. Porosity, both in the matrix and in the Ti(oxide) relics, was affected, and variations in pressure had a greater effect than variations in temperature (**figure 12**). The 'standard' pressing conditions of 1200°C and 14 MPa produced an acceptable structure with some fine porosity in the matrix and a moderate number of voids in the Ti(oxide) relics. The voids in both matrix and Ti(oxide) relics can be substantially eliminated by pressing at 1250°C and 21 MPa (**figure 12**).

The morphology of the microconstituents was also affected, with the Ti oxide in the matrix forming profuse, small, well-defined acicular crystallites at temperatures of 1200°C and below, but not at 1250°C (**figure 13**).

### 8.5 Effect of Metallic Getter

Two per cent titanium metal powder is normally added to scavenge excess oxygen from the powder compact and maintain reducing conditions during hot pressing. Generally, all the Ti is consumed during the process, but if added in excess amounts the Ti may not be fully oxidised (**figure 14**). The oxidation of the Ti is exothermic and incidentally augments the heating of the material. **Figure 15** shows an example of enhanced grain growth around Ti(oxide) relics. The Ti(oxide) relics also show evidence of reaction with the matrix (**figure**

**1a**) and a range of elements including Al, Ba, Cs and Fe have been detected in the relics, for examples see **figures 7** and **12a**.

In systematic experiments, where the Ti getter was eliminated or replaced by 2% Ni or 2% Fe, small needles of hibonite $Ca(TiAl)_{12}O_{19}$ [T.J. White, AAEC, personal communication] were present (**figure 16**) but absent with 2% Tl or 1.7% Al. These crystals are generally smaller and exhibit darker contrast than the acicular Ti oxide phase. It is not clear why reducing conditions should prevent the formation of hibonite.

## 9. DIFFUSION EFFECTS

Observation of the interaction of various inclusions with the Synroc matrix shows that during the hot-pressing operation, diffusion over ten micrometres or so is possible. Examples include the following:

(i) Diffusion of Ca and Ti into tramp zirconia fragments (**figure 3**).

(ii) Diffusion of Ba into Ti(oxide) relics (**figure 7**).

(iii) Diffusion of Al into Ti(oxide) relics (**figure 12a**).

(iv) Diffusion of Ti from relics into matrix (**figure 1a**).

(v) Diffusion of elements into and out of Synroc segregations (**figures 6b and 7**).

These observations give an indication of the scale below which inhomogeneities in the feed material should be unimportant.

## 10. DISCUSSION

The structure of Synroc C, a ceramic possibly comprised of up to 40 elements, is particularly complex. Apart from additives and unwanted contaminants and segregations, there are basically four major ceramic phases in this particular batch of Sandia Synroc. The phases are hollandite, zirconolite and perovskite which form a fine equi-axed matrix and a Ti oxide phase, based on rutile, which generally is slightly larger and varies from equi-axed grains through irregular needles to acicular crystals.

The factors determining the matrix Ti oxide morphology presumably include pressing temperature and composition as well as redox potential, but the fine grain size and the complex nature of the phase assemblage preclude a detailed study. This work has indicated that the sharp acicular crystallites are favoured by pressing temperatures of 1200°C and below. A further report in this series deals with some of the effects of composition [Stevens *et al.* 1987].

Many of the process variables cause characteristic effects on the microstructure. Microscopic examination can provide a guide to material quality. The detection and identification of serious Ca/Ba segregation, with associated cracking, is an example of the contribution of microscopy to the development of a successful Synroc process.

## 11. CONCLUSIONS

Some typical microstructures formed in Synroc C (Sandia RE15642), and revealed by optical and electron microscopy, have been described, and the effects on the microstructure of altering certain process variables have been reviewed.

Down to one micrometre, the microstructure, although particularly complex, is basically a dispersion of Ti oxide (or oxides) in a matrix of fine equi-axed grains of perovskite and, nominally, zirconolite and barium hollandite. The Ti oxide has a variable morphology with an acicular form favoured by pressing temperatures of 1200°C and below. Other acicular phases may also be present, such as hibonite (a calcium-aluminium titanate) which is favoured by less strongly reducing conditions. Pressing at temperatures approaching the melting point (*e.g.* 1290°C) leads to enhanced growth of the Ti oxide and colonies of coarse, aligned acicular crystals are formed.

Both the temperature and pressure of the pressing operation are important in controlling porosity, the pressure being more effective than temperature over the range 7 to 21 MPa and 1150°C and above. The microstructure is not critically dependent on the time of pressing.

## 12. ACKNOWLEDGEMENTS

The samples were prepared by J Woolfrey, B Seatonberry, C Quan and W Buykx. Most of the materials examined derive from the experiments of W Buykx.

## 13. REFERENCES

Cooper, J.A., Cousens, D.R., Lewis, R., Myhra, S., Segall, R.L., Smart, R St C., Turner, P.S., White, T.J. - [1985]. Microstructural characterization of Synroc C and E by electron microscopy. *J. Am Ceram. Soc.*, 68 (2)64-70.

Dosch, R.G., Headley, T.J., Hlava, P. - [1984]. Crystalline titanate ceramic nuclear waste forms: processing and microstructure. *J. Am. Ceram. Soc.*, 67 (5) 354-361.

Mendel, J.E., and seven other authors - [1977] Annual report on the characteristics of high-level waste glasses. BNWL-2252.

Ringwood, A.E. - [1978] Safe Disposal of High-level Nuclear Reactor Wastes: a New Strategy. ANU Press, Canberra.

Stevens, G.T., Watson, K.G., Bellrose, A [1987] - Microstructural aspects of Synroc from Sandia precursor. 2. Some effects of impurities. AAEC/E649.

**TABLE 1**
**TYPICAL COMPOSITION OF SYNROC B**

| Oxide | wt% |
|---|---|
| $TiO_2$ | 71.4 |
| $ZrO_2$ | 6.6 |
| $Al_2O_3$ | 5.4 |
| BaO | 5.6 |
| CaO | 11.0 |

**TABLE 2**
**TYPICAL SIMULATED HIGH-LEVEL WASTE COMPOSITION**

| Oxide | wt % | Oxide | wt % |
|---|---|---|---|
| $Cr_2O_3$ | 0.87 | $Ag_2O$ | 0.23 |
| $Fe_2O_3$ | 3.82 | CdO | 0.25 |
| NiO | 0.36 | $TeO_2$ | 1.84 |
| $P_2O_5$ | 1.70 | $Cs_2O$ | 7.28 |
| $Rb_2O$ | 0.90 | BaO | 3.97 |
| SrO | 2.67 | $La_2O_3$ | 8.41 |
| $Y_2O_3$ | 1.51 | $Pr_6O_{11}$ | 3.75 |
| $ZrO_2$ | 12.51 | $Nd_2O_3$ | 11.74 |
| $MoO_3$ | 13.08 | $Sm_2O_3$ | 2.33 |
| $RuO_2$ | 7.52 | $Eu_2O_3$ | 0.51 |
| $Rh_2O_3$ | 1.21 | $Gd_2O_3$ | 0.91 |
| PdO | 3.75 | $U_3O_8$ | 5.16 |

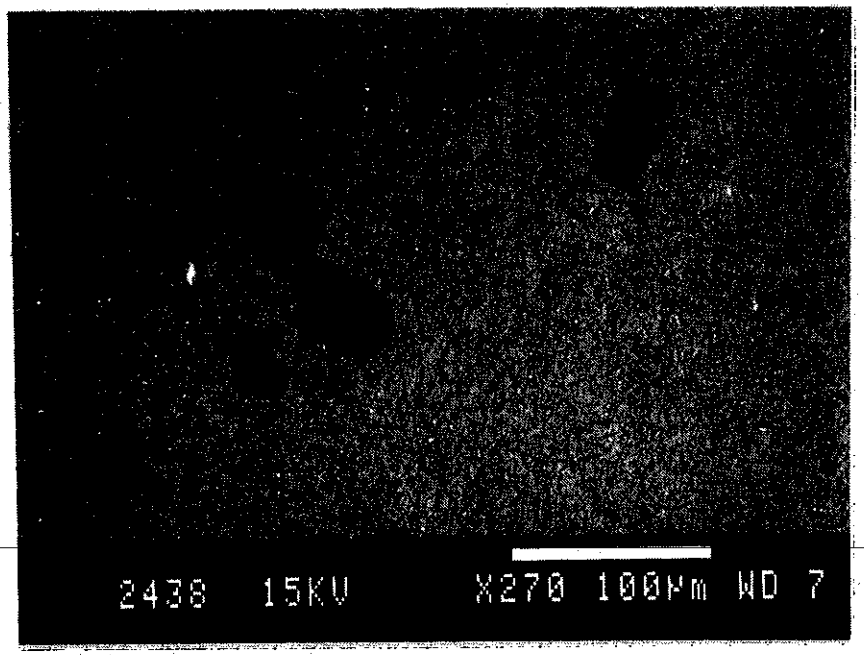


(a) SEM micrograph showing the oxide relics of the Ti metal addition in the Synroc matrix.

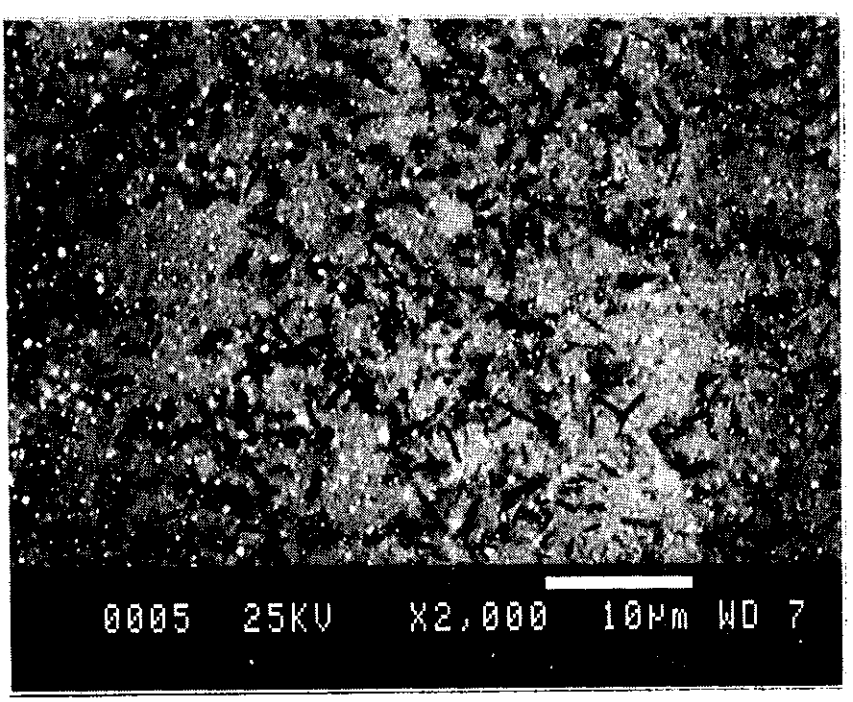


(b) SEM micrograph showing the morphology of the Synroc C phases.

Figure 1 Representative microstructures of Synroc C from Sandia RE15642 precursor hot-pressed for 2 h at 1200°C.

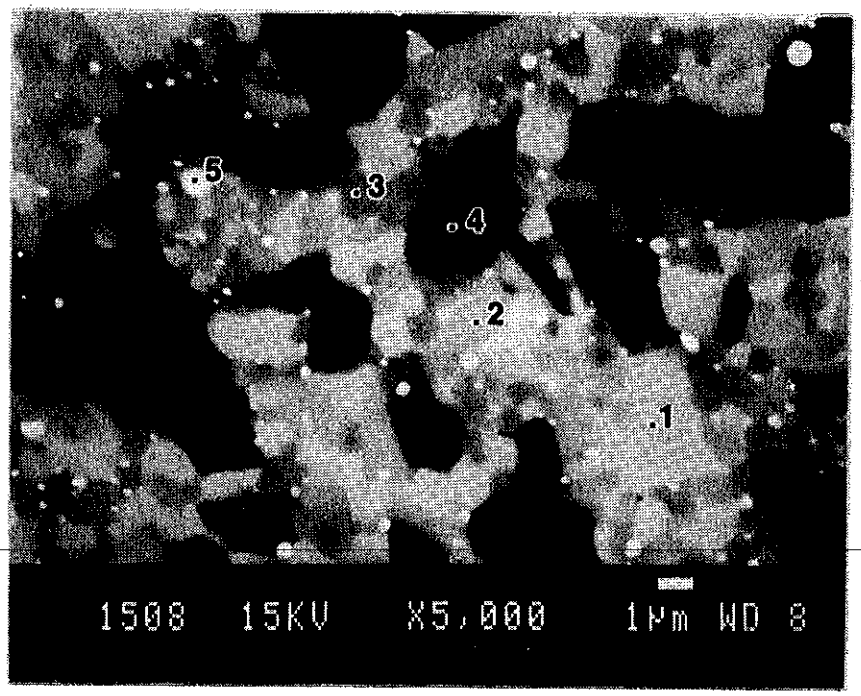


(a) SEM micrograph showing regions selected for EDS. Sample hot-pressed for 2 h at 1320° C.

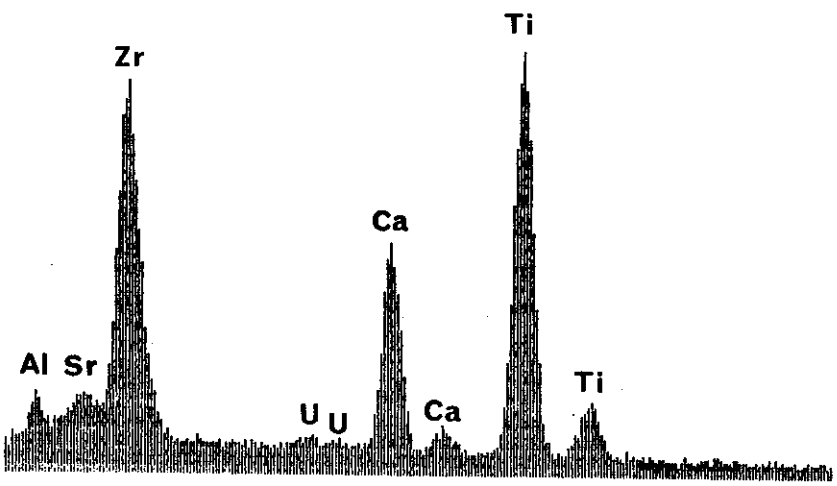


(b) XES spectrum from region 1 - zirconolite.

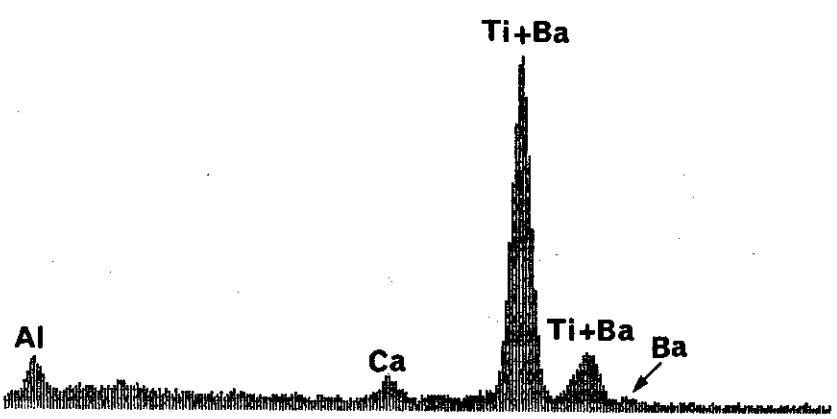


(c) XES spectrum from region 2 - hollandite.
The Ba lines are almost entirely obscured by the Ti lines,
but pronounced asymmetry is apparent in the smaller β line.

Figures 2a-g Identification of the Synroc C phase regions.

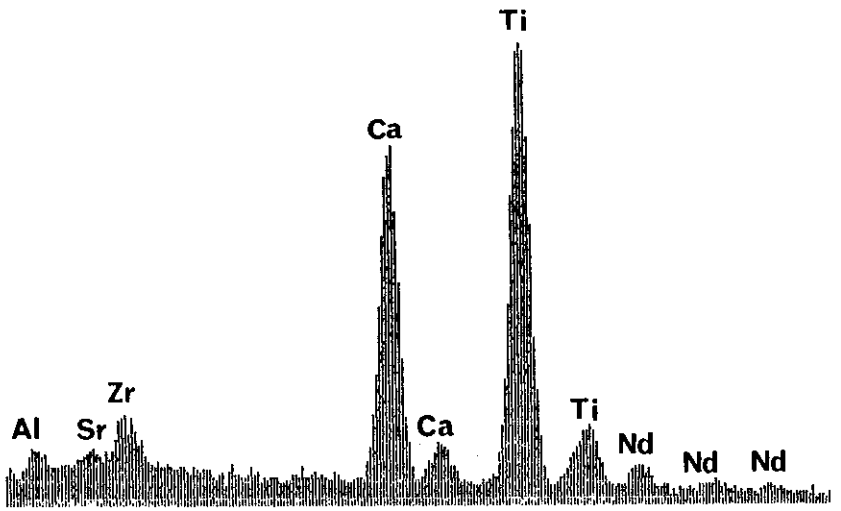


(d) XES spectrum from region 3 - perovskite.

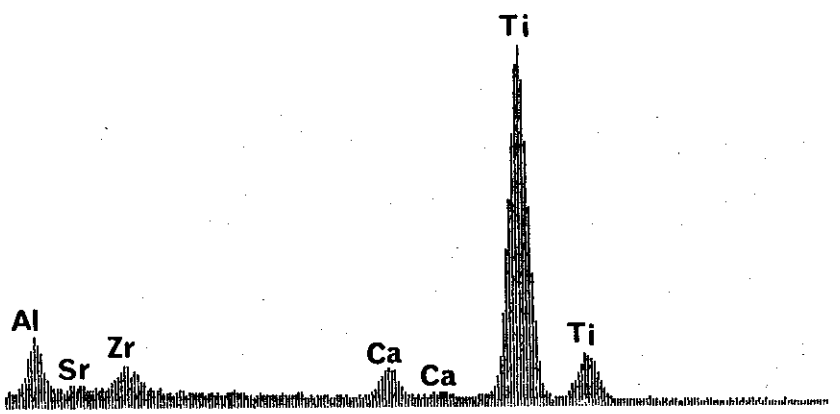


(e) XES spectrum from region 4 - rutile.

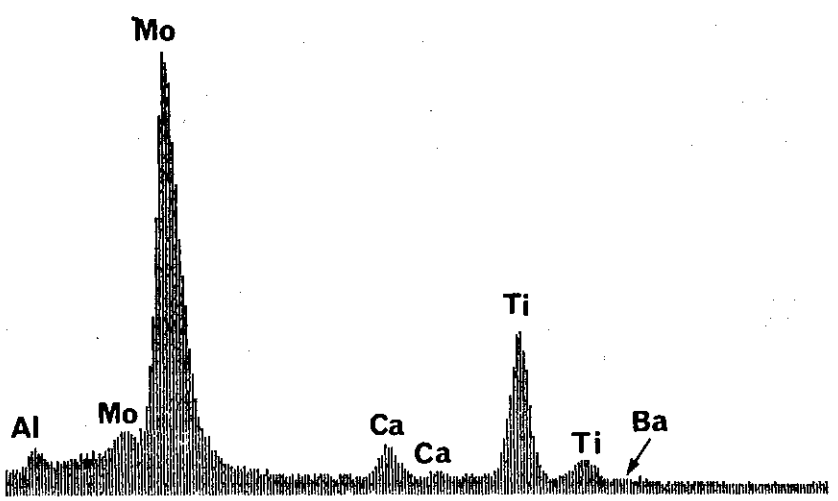


(f) XES spectrum from region 5 - metallic alloy.

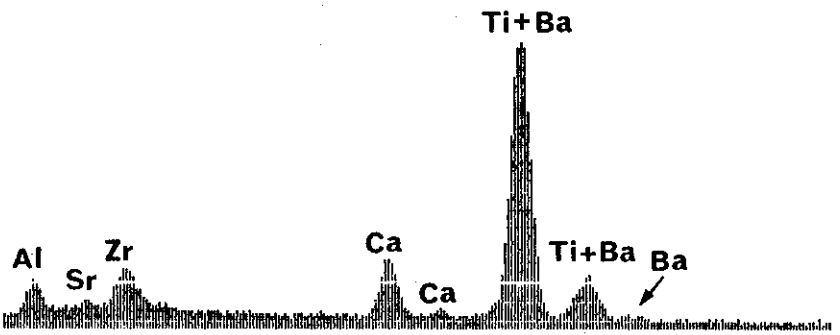


(g) XES spectrum from scan of field shown in (a).


Figure 3 Some inclusions in Synroc C. Sample hot-pressed for 2 h at 1280°C.

C - calcium-rich segregation; R - titanium (oxide) relic; Z - zirconia fragment from attriter. Note the rim of metallic particles on the outside of the halo around the zirconia fragment. The rim defines the original size of the particle. The halo is formed by Ti and Ca diffusing in from the matrix. Minimum halo width is about 4 micrometres.

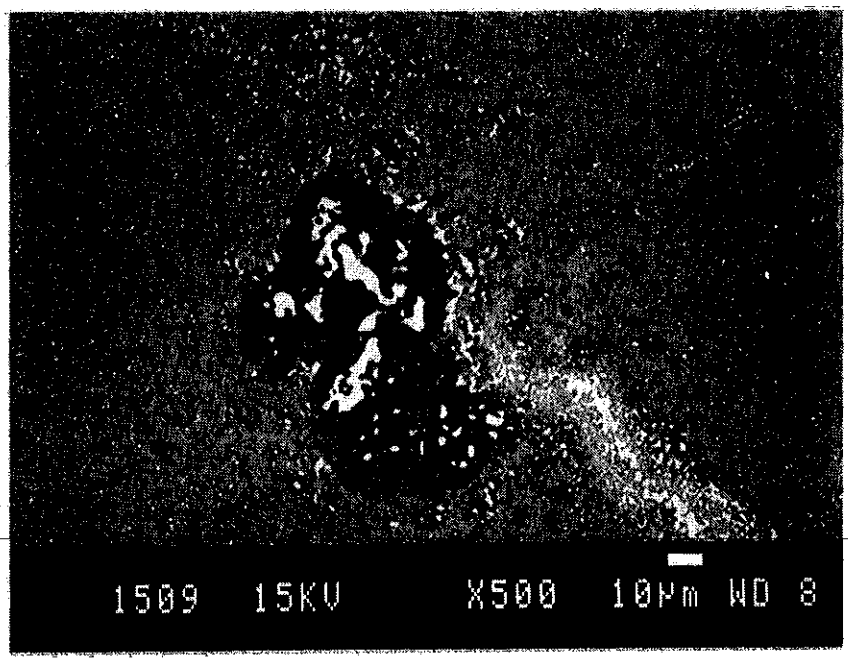


Figure 4 Interaction of stainless steel contamination with Synroc C matrix and Ti(oxide) relic. Sample hot-pressed for 2 h at 1200°C.

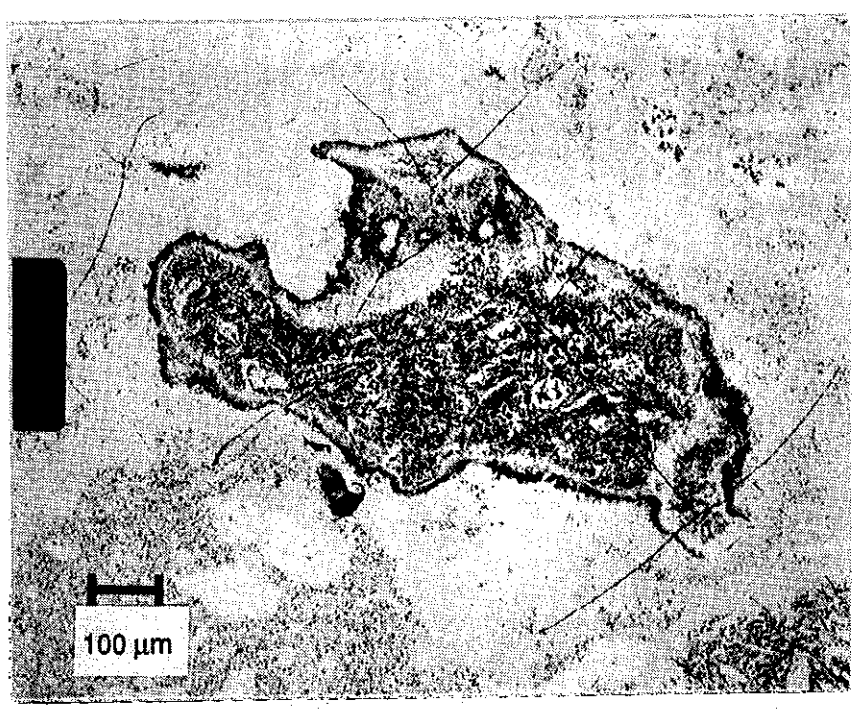


(a) Optical micrograph, bright field illumination. Showing internal cracking extending into surrounding matrix.

Figure 5 Calcium/barium segregation in Synroc C.

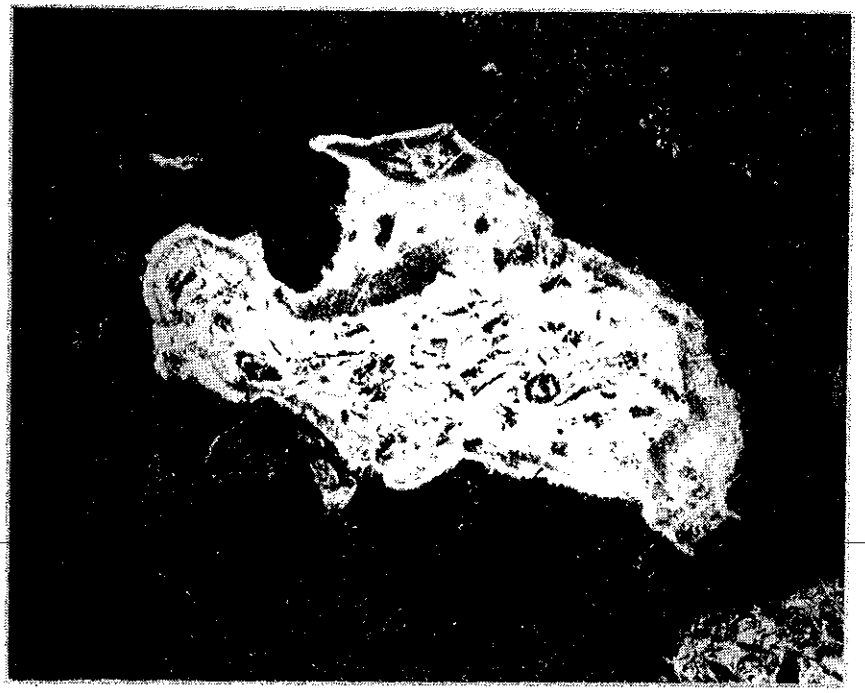

(b) Optical micrograph, dark field illumination. Showing internal reflection of components in segregation.

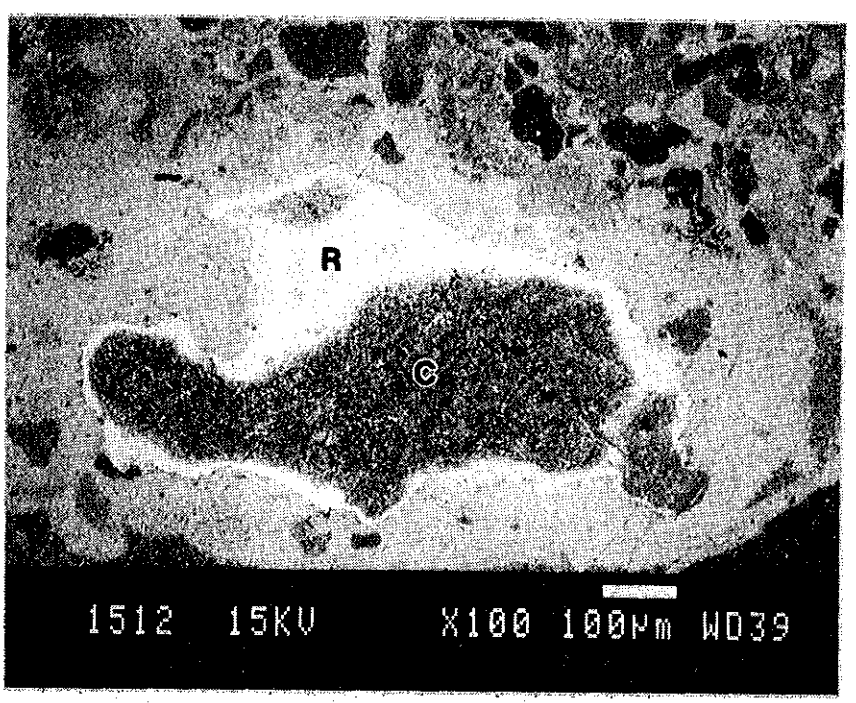


(c) SEM micrograph, BSE imaging. Showing composition dependent contrast. High atomic number light, low atomic number dark.

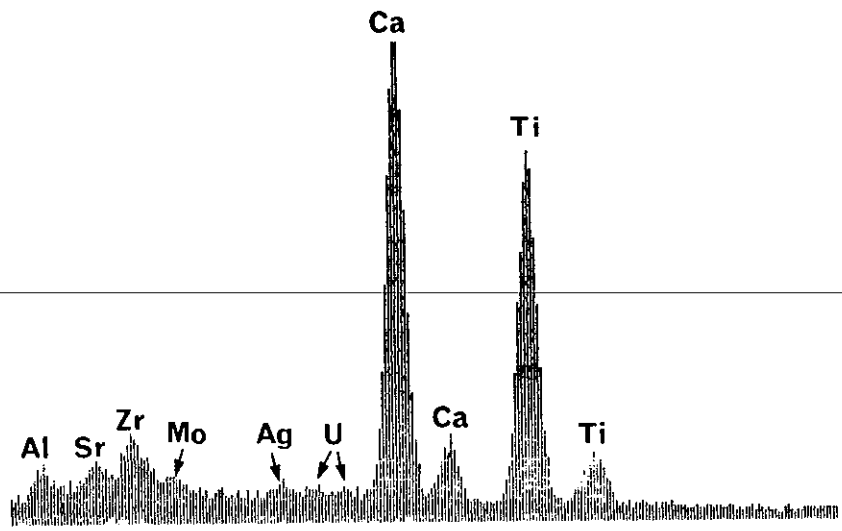


(d) XES spectra from core of segregation (labelled C in SEM micrograph). Note high Ca content.

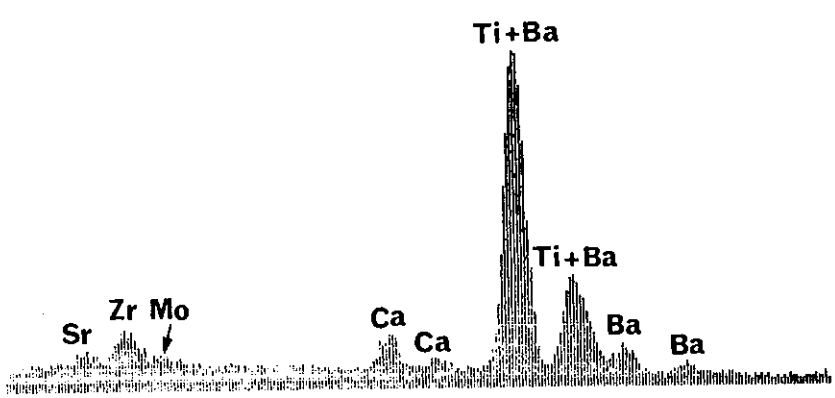


(e) XES spectra from rim of segregation (labelled R in SEM micrograph). Note high Ba content.

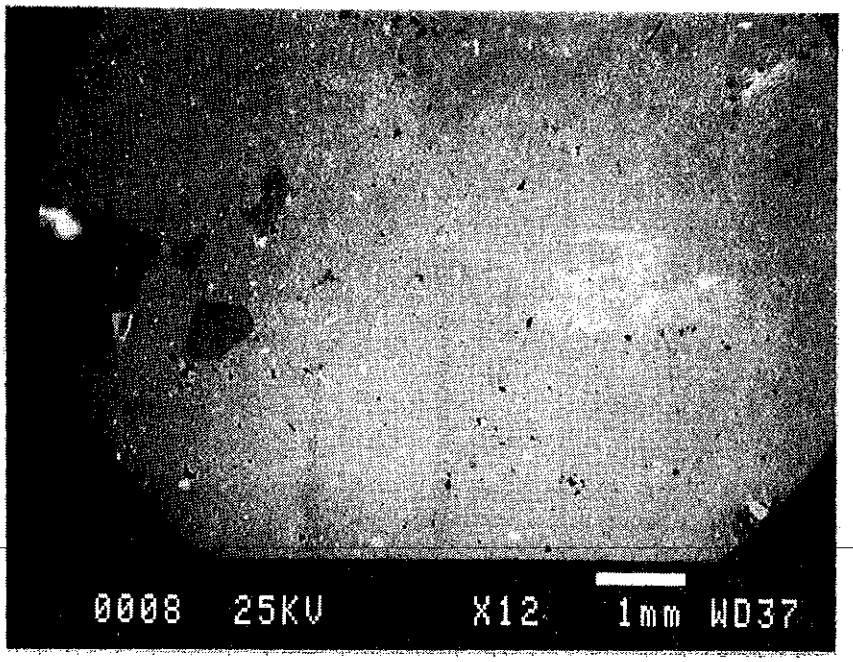


(a) Material sieved before calcination. Note large segregations up to 2 mm in size.

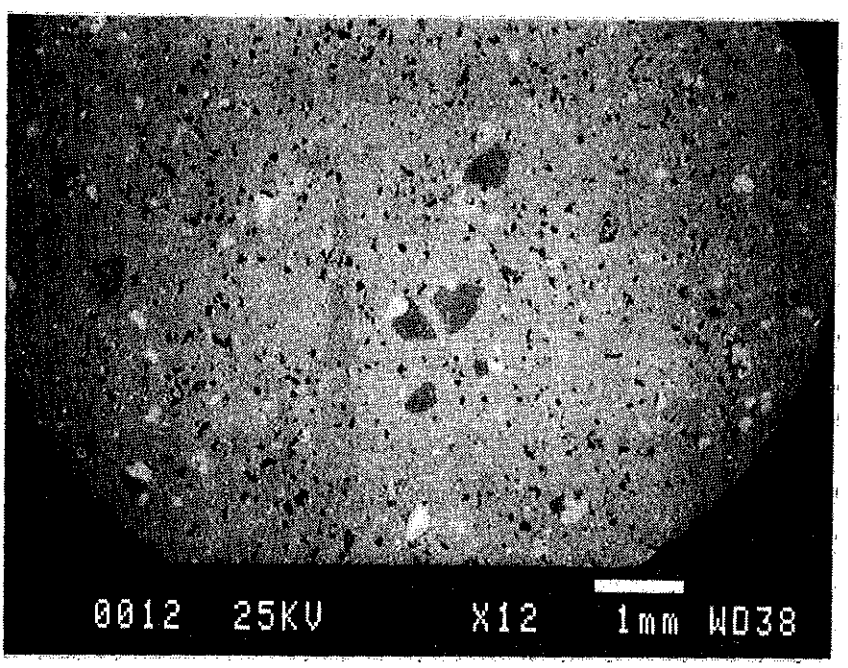


(b) Material hammer-milled before calcination. The segregates are reduced to about 0.5 mm in size. The light regions are high in Ba while the darker regions are higher in Ti and Al than the matrix.

Figure 6 Segregation in Synroc C. Effect of hammer-milling.

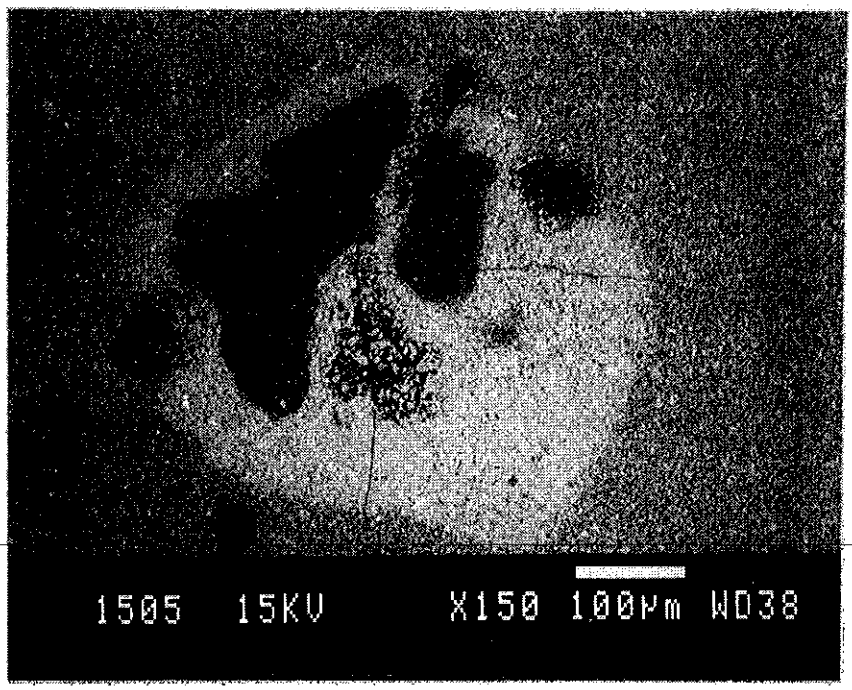


Figure 7 Interaction of calcium segregation with matrix and Ti(oxide) relics. Comparison of XES spectra shows this segregation to consist of a high Ca core into which Ti has diffused from the matrix, leaving a zone high in Ba which in turn has reacted with Ti(oxide) relics.

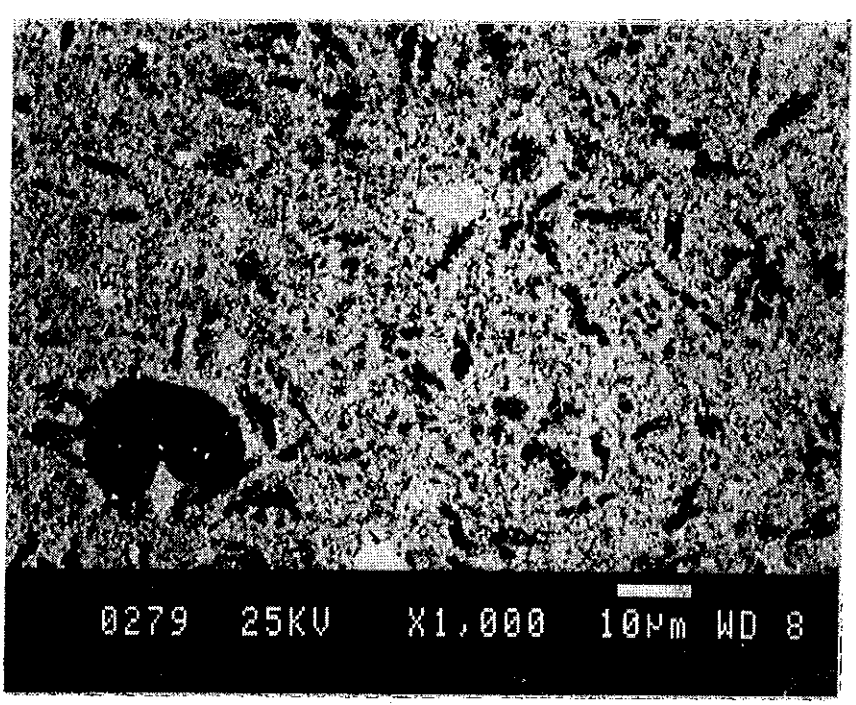


Figure 8 Microstructure of Synroc C when pure hydrogen was the inlet gas for the calciner.

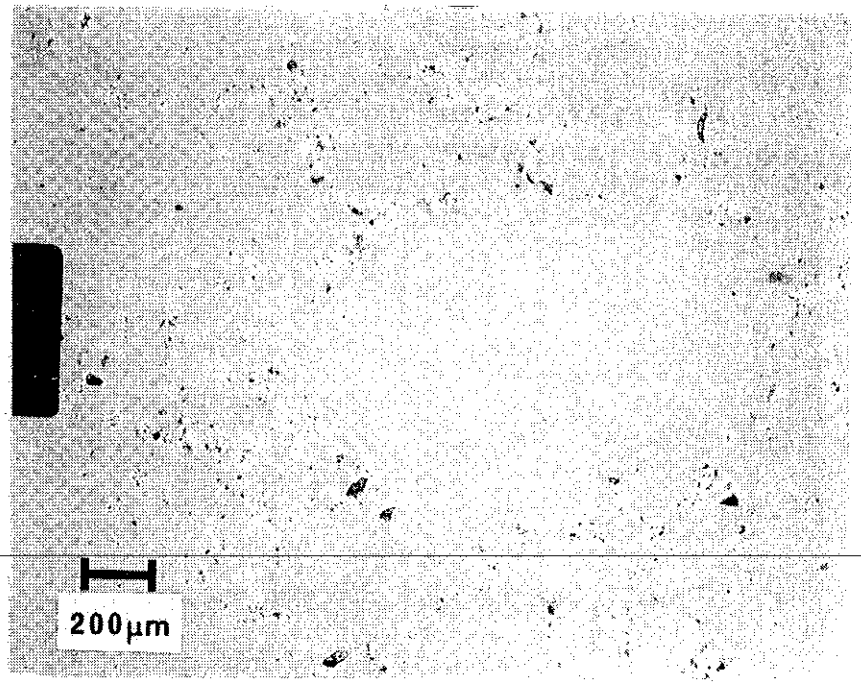


(a) Pressure applied immediately 1200°C was reached.

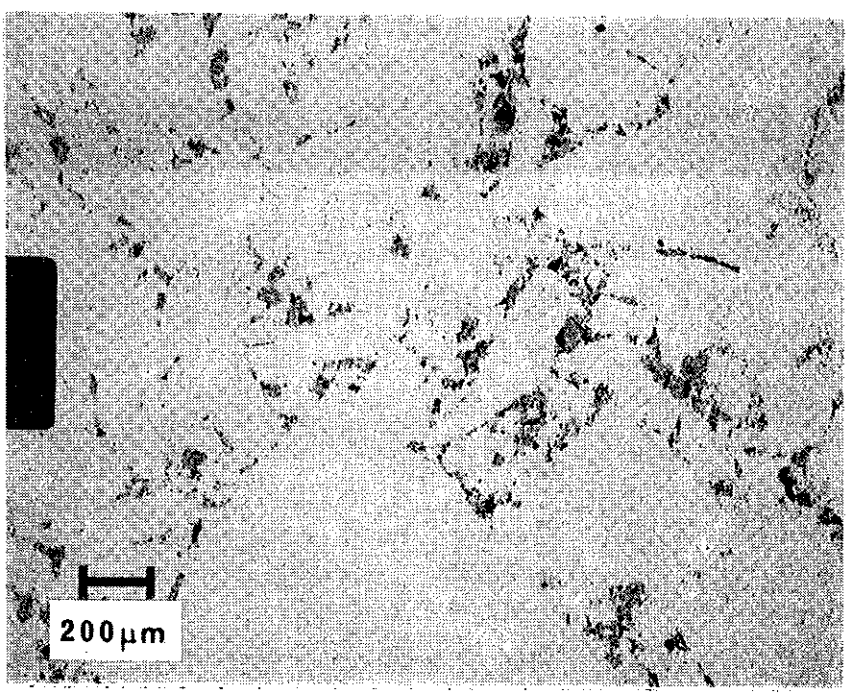


(b) Specimen soaked at 1200°C for 4 h before application of pressure.

Figure 9 Optical micrographs showing porosity around dense granules of Synroc hot-pressed at 1200°C for 2 h

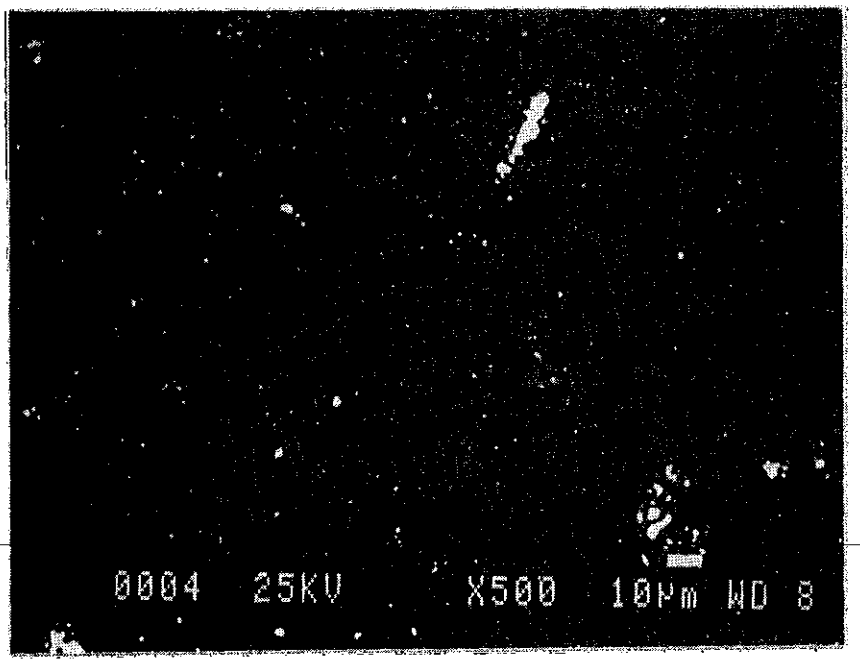


Figure 10 Colonies of large crystals of Ti oxide produced at 1290°C.


Figure 11 Large crystals of Ti oxide produced at 1300°C.

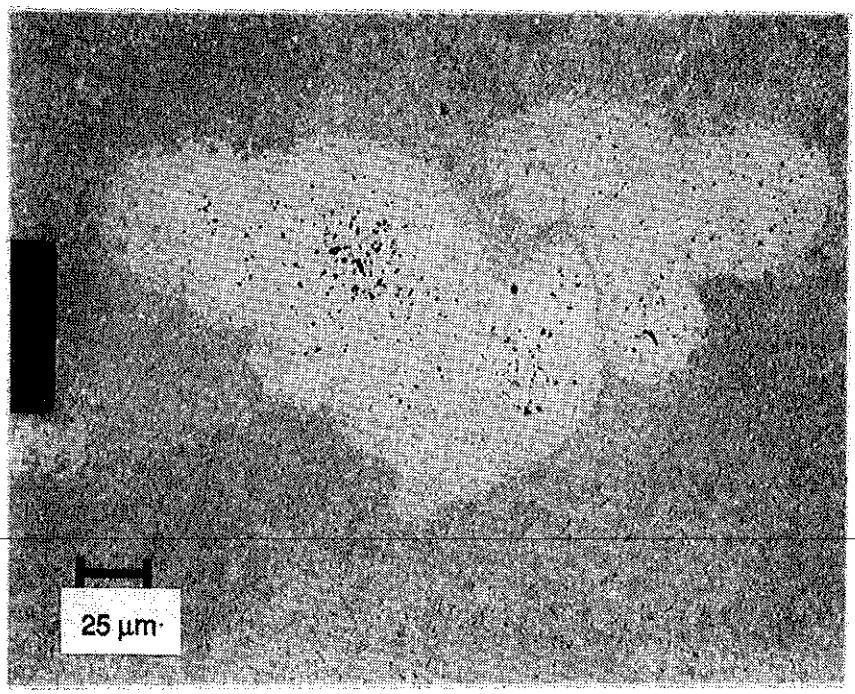


(a) Hot-pressed at 1250°C and 14 MPa. Depicts reaction zone, internal porosity and banding in Ti(oxide) relic. The darker bands have a higher Al content than the lighter material.

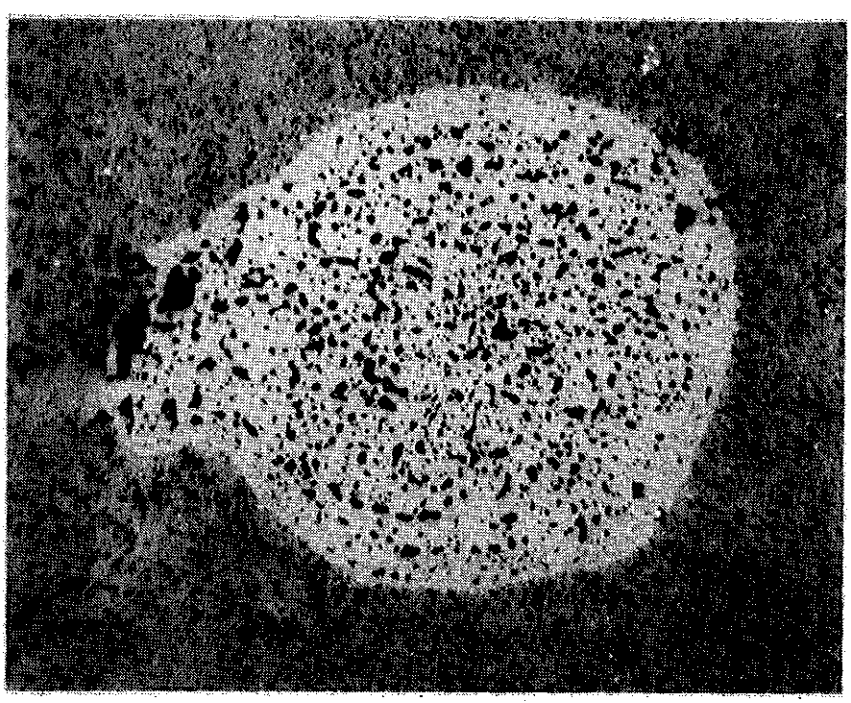

(b) Hot-pressed at 1250°C and 7 MPa. Depicts gross porosity in Ti(oxide) relic and matrix.

Figure 12 Optical micrograph showing voids in Ti(oxide) relic and surrounding Synroc matrix.

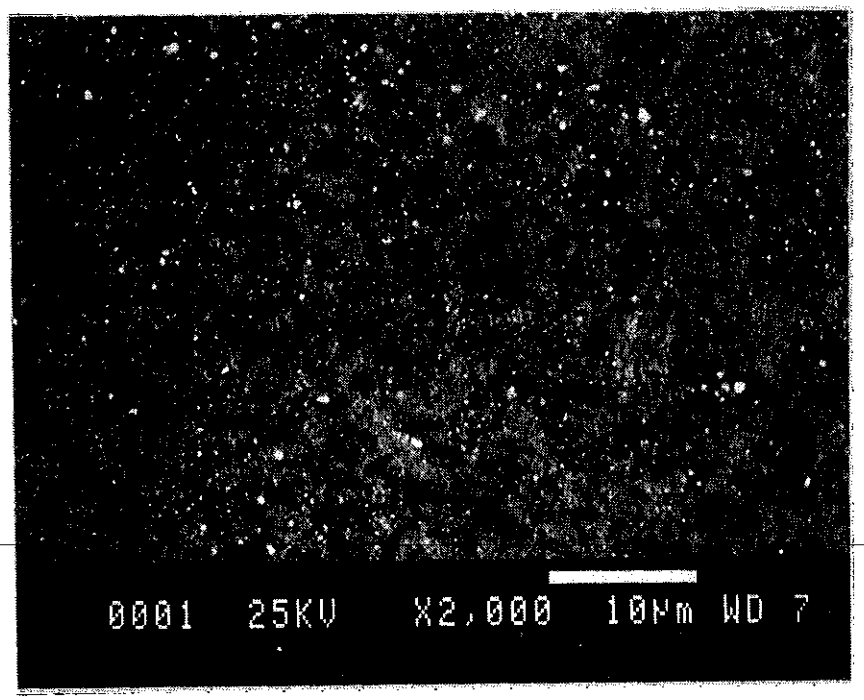


(a) Hot-pressed at 1150°C and 21 MPa.

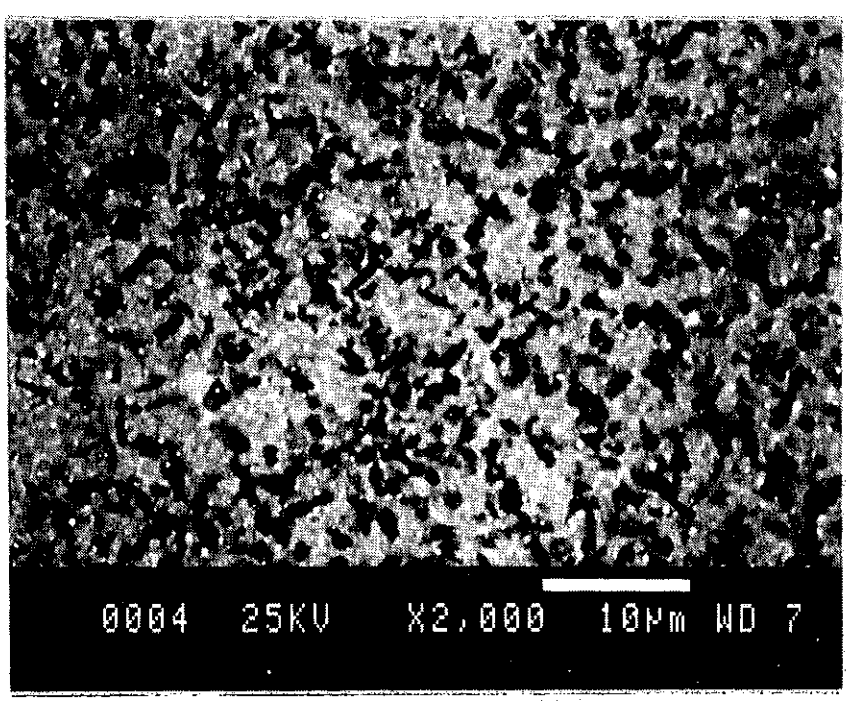


(b) Hot-pressed at 1250°C and 21 MPa.

Figure 13 Effect of pressing temperature on microstructure.

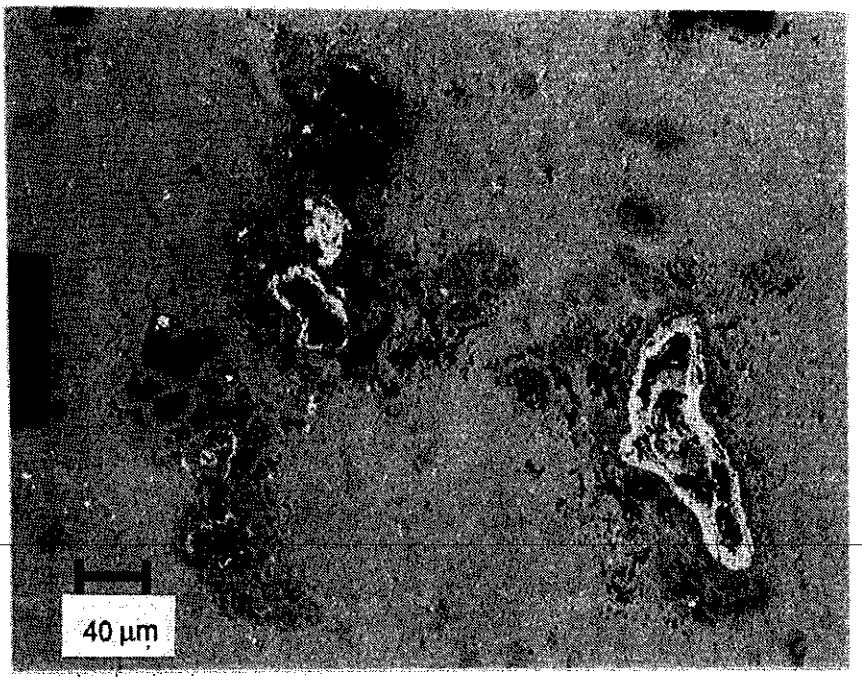


Figure 14 Optical micrograph of cluster of Ti(oxide) relics and voids in Synroc pressed with 4% metallic Ti getter. Some relics are not fully oxidised and exhibit metallic lustre.

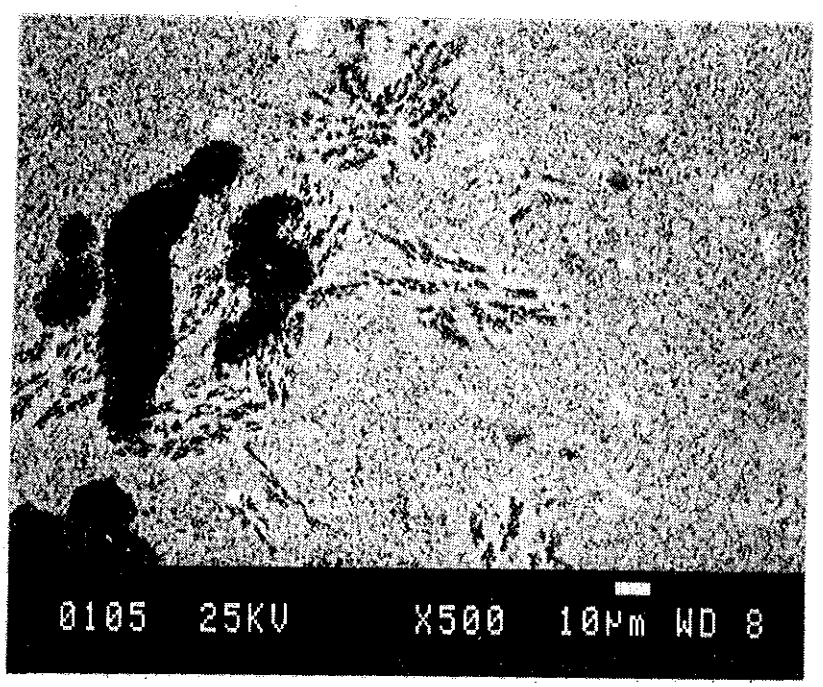


Figure 15 Enhanced Ti oxide crystal growth around Ti(oxide) relics.

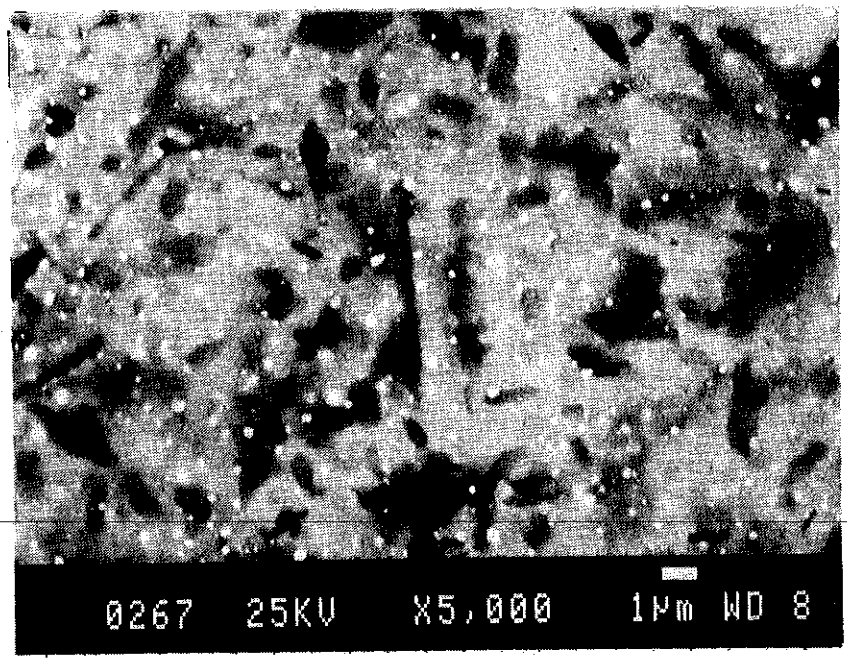


Figure 16 Small crystals of a calcium-aluminium titanate (probably hibonite $Ca(TiAl)_{12}O_{19}$, T J White, AAEC, personal communication).